Dark-state optical potential barriers with nanoscale spacing

Wenchao Ge and M. Suhail Zubairy
Institute for Quantum Science and Engineering (IQSE) and Department of Physics and Astronomy, Texas A&M University, College Station, Texas 77843-4242, USA

(Received 14 August 2019; accepted 14 January 2020; published 5 February 2020)

Optical potentials have been a versatile tool for the study of atomic motions and many-body interactions in cold atoms. Recently, optical subwavelength single barriers were proposed to enhance the atomic interaction energy scale, which is based on nonadiabatic corrections to Born-Oppenheimer potentials. Here we present a study for creating an alternative landscape of nonadiabatic potentials—multiple barriers with subwavelength spacing at tens of nanometers. To realize these potentials, spatially rapid-varying dark states of atomic Λ configurations are formed by controlling the spatial intensities of the driving lasers. As an application, we show that bound states of very long lifetimes on the order of seconds can be realized. Imperfections and experimental realizations of the multiple barriers are also discussed.

DOI: 10.1103/PhysRevA.101.023403

I. INTRODUCTION

Optical potentials have been a very useful tool for manipulation of atomic motions, such as simulation of many-body physics [1,2]. The typical potentials can be generated using a far-detuned light through optical dipole force due to a spatially varying ac-Stark shift [3]. The potential landscape is therefore determined by the spatial variation of the light intensity. Except operating near the surface [4–9] or using special masks [10,11], the spatial intensity variation is often limited by the wavelength λ of the light. To realize subwavelength resolution in the far field, various approaches have been proposed [12–33], such as multitone dressing [18–20], multiphoton processes [21–24], and atomic dark states in Λ configurations [25–33].

Recently, a novel idea of subwavelength optical potentials was proposed by considering the nonadiabatic corrections [34] to the spatially varying dark states in Λ configurations [35,36]. A subwavelength potential barrier arises when the kinetic energy of an atom experiences a rapid change of its internal state in a subwavelength region. This type of optical potential is drastically different from the optical dipole potentials as the former is purely quantum mechanical since the potential energy is proportional to $\hbar$. The first experiment of these barriers has been demonstrated [37]. By using standing waves, the potentials can form lattices with subwavelength barriers spaced by $\lambda/2$. With time-dependent engineering of the lattices, smaller spacings between narrow barriers are possible [38–40]. However, heating can arise and the dark-state lifetime can be limited due to lattice modulation [39,40].

In this paper, we present a method to create multibarrier nonadiabatic potentials with subwavelength spacing, realizing a type of optical potential landscape without time-dependent modulations. Our idea is based on dark-state nonadiabatic potentials of three-level atoms in Λ configurations [Fig. 1(a)] by controlling the spatial intensity variations on the driving lasers. We employ the Born-Oppenheimer (BO) approximation [34] to study the internal eigenstates of the atoms and nonadiabatic corrections from the atomic motions. We derive the general formula for the corrections of an arbitrary spatial intensity function. In particular, we show that double barriers and triple barriers with subwavelength spacings can be realized.

Double-barrier potentials have been widely studied in solid-state systems, such as semiconductor heterostructures [41–43]. They are important for understanding effects such as resonant tunneling [42] and quasibound states [44]. Our scheme offers a platform to study double barriers in cold atoms in the subwavelength regime, where many-body atomic interactions can be strongly enhanced. As an example, we illustrate the formation of bound states of two and three atoms via magnetic dipolar interactions numerically. Our results show that the double-barrier potentials can support bound states of very long lifetimes on the order of seconds.

II. DARK-STATE TRAPPING AND NONADIABATIC POTENTIALS

We consider three-level atoms with a Λ energy structure shown in Fig. 1(a). The two ground states $|g_1\rangle$ and $|g_2\rangle$ are long lived, which can be hyperfine-split metastable states or Zeeman sublevels [45], and an excited state $|e\rangle$ has a spontaneous decay rate γ. The total Hamiltonian of the system includes the kinetic energy and the internal atomic interaction is given by [35] $\mathcal{H} = \frac{p^2}{2m} + \mathcal{H}_{\rm in}$, where

$$\mathcal{H}_{\rm in} = -\hbar\Delta\,|e\rangle\langle e| + \left[\hbar\frac{\Omega_c(x)}{2}\,|e\rangle\langle g_1| + \hbar\frac{\Omega_p(x)}{2}\,|e\rangle\langle g_2| + \text{H.c.}\right]. \quad (1)$$

Here $\Omega_c(x)$ [$\Omega_p(x)$] is the spatial-dependent Rabi frequency of the off-resonant coupling (probe) field for the transition between $|e\rangle$ and $|g_1\rangle$ ($|g_2\rangle$) with a detuning Δ. These fields form a resonant Raman transition between the ground states [46]. To study the nonadiabatic corrections, we will employ a similar procedure to that in Ref. [36]. However, in contrast

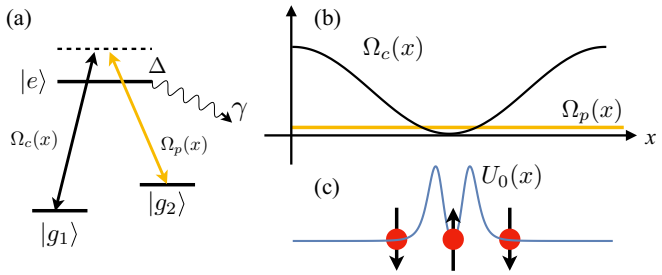

FIG. 1. Schematic of our scheme. (a) Atomic configuration and the coupling to two lasers. An example of (b) spatial dependencies for $\Omega_c(x)$ and $\Omega_p(x)$ and (c) the corresponding nonadiabatic potential. The circular disks represent atoms and the arrows represent the population of dark-state atoms.

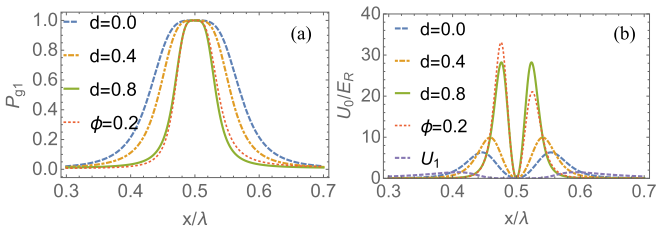

FIG. 2. (a) Dark-state population of $|g_1\rangle$ for double-barrier potentials as a function of x/λ in one period, and (b) the corresponding nonadiabatic potentials of double barriers with subwavelength spacings for $d = 0,\ 0.4\,,0.8$ at $\phi = 0$, and $d = 0.8$ at $\phi = 0.2$ with $\epsilon = 1/10$. A component of the nonadiabatic potential for the bright states (U_1, the dashed curve) is plotted in (b) for $d = 0$ and $\phi = 0$.

to previous works [35–39], we consider both the coupling and the probe fields to be position dependent, which will lead to general expressions of the nonadiabatic corrections.

We are interested in the limit of slow atomic motions such that the energy of the external motion (the kinetic energy and the potential) is much smaller than the internal energy scale determined by $\mathcal{H}_{\rm in}$. Within this limit, we can apply the BO approximation [34] to treat the internal Hamiltonian separately. The validity of this limit will be discussed later. We can diagonalize $\mathcal{H}_{\rm in}$ and obtain the eigenstates to be

$$|D(x)\rangle = \frac{-\Omega_p(x)\,|g_1\rangle + \Omega_c(x)\,|g_2\rangle}{\Omega(x)},$$
$$|B_\pm(x)\rangle = \frac{\Omega_c(x)\,|g_1\rangle + \Omega_p(x)\,|g_2\rangle + \Omega_\pm(x)\,|e\rangle}{\sqrt{\Omega^2(x)+\Omega_\pm^2(x)}}, \quad (2)$$

where the corresponding eigenenergies are 0 and $\hbar\Omega_\pm/2$, respectively. Here $\Omega(x) = \sqrt{\Omega_c^2(x)+\Omega_p^2(x)}$, $\Omega_\pm(x) = -\Delta \pm \sqrt{\Omega^2(x)+\Delta^2}$. Therefore, the atoms are trapped at the spatially varying dark state $|D(x)\rangle$ and are decoupled from the laser fields [26–29].

Since the momentum p and the position x do not commute, additional contributions arise when we diagonalize the kinetic energy using the position-dependent eigenbasis, which are termed as nonadiabatic corrections or geometric potentials [35,36]. To see this, we consider the unitary operator [36] $\mathcal{R} = |D(x)\rangle\langle D_0| + |B_+(x)\rangle\langle B_{+0}| + |B_-(x)\rangle\langle B_{-0}|$, where $|D_0\rangle$ and $|B_{\pm0}\rangle$ are the eigenstates located at a fixed position x_0. By applying the transformation, we obtain

$$\widetilde{\mathcal{H}} = \mathcal{R}^\dagger\mathcal{H}\mathcal{R} = \frac{(p-\mathcal{A})^2}{2m} + \sum_{a=\pm}\hbar\frac{\Omega_a(x)}{2}\,|B_{a0}\rangle\langle B_{a0}|, \quad (3)$$

where the effective vector potential $\mathcal{A} \equiv \hbar\mathcal{R}^\dagger\partial_x\mathcal{R} = i\hbar\alpha'(x)\sum_{a=\pm}N_a(|B_{a0}\rangle\langle D_0| - |D_0\rangle\langle B_{a0}|) + i\hbar\frac{\Omega'(x)}{\Omega(x)}C(|B_{-0}\rangle\langle B_{+0}| - |B_{+0}\rangle\langle B_{-0}|)$ with $\alpha(x) = \arctan[\Omega_p(x)/\Omega_c(x)]$, $N_\pm = 1/\sqrt{1+\Omega_\pm^2(x)/\Omega^2(x)}$, and $C = (\Delta\Omega/2)/(\Delta^2+\Omega^2)$. Therefore, we arrive at

$$\widetilde{\mathcal{H}} = \frac{p^2}{2m} + U_0(x)|D_0\rangle\langle D_0| + \sum_{a=\pm}\left(\hbar\frac{\Omega_a(x)}{2} + U_a(x)\right)|B_{a0}\rangle\langle B_{a0}| + \mathcal{V}, \quad (4)$$

where the nonadiabatic potential for the dark state is [35]

$$U_0(x) = \frac{\hbar^2}{2m}[\alpha'(x)]^2. \quad (5)$$

It is the nonzero derivative of $\alpha(x)$ that gives rise to potential barriers (positive potential) for the dark state $|D(x)\rangle$. Thus the ratio of the two driving lasers, $f(x) \equiv \Omega_c(x)/\Omega_p(x) = \tan[\alpha(x)]$, plays an important role in engineering interesting spatial structures of subwavelength barriers. The nonadiabatic potentials for the bright states are $U_a = \hbar^2/(2m)[N_a^2\alpha'^2(x) + C^2\Omega'^2(x)/\Omega^2(x)] = N_a^2U_0(x) + 4C^2U_1(x) \leqslant U_0(x) + U_1(x)/4$, where $U_1(x) = \hbar^2/(8m)\Omega'^2(x)/\Omega^2(x)$. The off-diagonal contribution that couples between the eigenstates is given by

$$\mathcal{V} = -\frac{p\mathcal{A}}{2m} + U_b(x)\,|B_{+0}\rangle\langle B_{-0}| + \sum_{a=\pm}U_{0a}(x)\,|D_0\rangle\langle B_{a0}| + \text{H.c.}, \quad (6)$$

where $U_b(x) = \hbar^2/(2m)N_+N_-\alpha'^2(x)$ and $U_{0a} = \pm\hbar^2/(2m)N_\mp C\alpha'(x)\Omega'(x)/\Omega(x)$. The coupling rates between the dark state and the bright states are $V_{\pm D} \equiv |\langle B_{\pm0}|\mathcal{V}|D_0\rangle|/\hbar = |U_{0\pm}(x)|/\hbar$, which determine the loss rate of atoms out of the dark state. We show that $U_b(x) \leqslant U_0(x)/2$ and $|U_{0\pm}(x)| \leqslant \sqrt{U_0(x)U_1(x)}/2$. To ensure the validity of the BO approximation,

$$U_i(x)/\hbar \ll |\Omega_\pm(x)| \quad (i = 0, 1). \quad (7)$$

In particular, as shown numerically in Fig. 2(b), $U_1(x) \lesssim U_0(x)$ around the double barriers. For $|\Delta| \lesssim |\Omega(x)|$, we can reduce Eq. (7) to $U_0(x) \ll \hbar|\Omega(x)|$. Under this condition, the off-diagonal coupling $\mathcal{V}$ is far detuned from the energy spacing between the eigenstates, therefore it can be treated as a perturbation. Then the excitation to the open channels can be estimated [36,46] as $P_B \sim |\langle B_{a0}|\mathcal{V}|D_0\rangle|^2/\Omega^2(x) = V_{\pm D}^2/\Omega^2(x) \ll 1$. The effective loss rate of the dark state atoms is given by $\gamma_d \sim \gamma V_{\pm D}^2/\Omega^2(x)$. A more rigorous result of the dark-state decay rate is calculated from the corrections to the dispersion of atoms in the Bloch bands [35], which shows a similar relation to our perturbative result.

III. SUBWAVELENGTH OPTICAL POTENTIALS

The nonadiabatic potential arises due to the rapidly spatial change of the internal dark state. Previous studies [35–40,47] have focused on the situation when the ratio of the coupling laser to the driving laser is an approximated linear function near certain values, i.e., $f(x) \approx kx/\epsilon$ for $|kx| \lesssim \epsilon$. The nonadiabatic potential for the dark state is given by [36] $U_0(x) = \frac{\hbar^2 k^2}{2m\epsilon^2}/[1 + (kx/\epsilon)^2]^2$, which shows a single potential barrier located at $x = 0$ with $U_0(0) = \frac{\hbar^2 k^2}{2m\epsilon^2}$ and a width $\Delta x \sim \epsilon/k$. In general, $f(x)$ can be made periodic, e.g., $f(x) = \sin(kx)/\epsilon$ [35,37], so the separation between two barriers is $\lambda/2$. Recent studies show that the separation can be reduced further via Floquet engineering [38–40].

Here we consider a more general situation of laser intensities as

$$f(x) = \frac{\Omega_c(x)}{\Omega_p(x)} = \frac{a + b\cos(kx)}{c + d\cos(kx + \phi)}, \tag{8}$$

which can be formed by a combination of standing waves and propagating waves. Here a, b, c, d, are the amplitude coefficients to be determined and ϕ is the phase control.

A. Double barrier with subwavelength spacing

We study spatial engineering of the Rabi frequencies to realize nonadiabatic multiple barriers with subwavelength spacing. The basic idea is to design a spatial function $f(x)$ such that its derivative is zero at $x = x_{\min}$ but quickly reaches its maximum in a subwavelength region away from $x_{\min}$.

We consider the situation for generating double barriers using

$$f(x) = \frac{1}{\epsilon}\frac{1 + \cos(kx)}{1 + d\cos(kx + \phi)}, \tag{9}$$

where $d < 1$. Here we take $\Omega_c(x) = \Omega_0[1 + \cos(kx)]$ and $\Omega_p(x) = \Omega_0\epsilon[1 + d\cos(kx)]$.

At $\phi = 0$, we find that the potential features are prominent at $kx \sim \pi$ and we arrive at

$$\alpha'(x) \approx \frac{k}{\epsilon(1-d)}\frac{k\delta x}{1 + \left[\frac{k^2\delta x^2}{2\epsilon(1-d)}\right]^2}, \tag{10}$$

where $\delta x = x - \pi/k$. The spatial function of the nonadiabatic potential $U_0(x)$ can be obtained from Eq. (5) by substituting the above relation of $\alpha'(x)$, from which we obtain three important features:

(1) $U_0(x_{\min}) = 0$ with $x_{\min} = \pi/k$.

(2) Two barrier peaks located around $x_{\max} = \pi/k \pm (4/3)^{1/4}\frac{\sqrt{\epsilon(1-d)}}{k}$ with $U_0(x_{\max}) = \frac{\hbar^2 k^2}{2m}\frac{\sqrt{27}}{8\epsilon(1-d)}$.

(3) We get a nonadiabatic potential well with a subwavelength width at half maximum to be $\Delta x \approx 0.2\sqrt{\epsilon(1-d)}\lambda$.

Furthermore, we study spatial variation on the population of one of the ground states, e.g., $P_{g_1}(x) = \frac{1}{1+f^2(x)}$. The nonadiabatic potential $U_0(x) \propto (\partial P_{g_1}(x)/\partial x)^2$, meaning that it is due to the rapid change of the population as a function of position such that the atoms cannot adjust its internal state adiabatically. In particular, $\partial P_{g_1}(x)/\partial x \propto f'(x) = 0$ at $x = k/\pi$, which corresponds to the dip in the nonadiabatic potential.

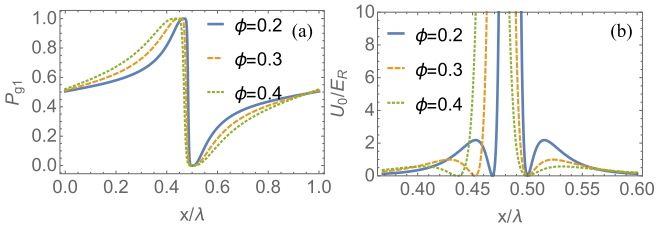

FIG. 3. (a) Dark-state population of $|g_1\rangle$ for creating triple-barrier potentials as a function of x/λ, and (b) the corresponding nonadiabatic potentials of triple barriers with subwavelength spacings for different values of ϕ. The inset magnifies the dashed-box area to show the triple-barrier feature.

We plot the numerical results of the ground-state population P_{g_1} and the double-barrier potential $U_0(x)$ for $d = 0$, 0.4, 0.8 at $\phi = 0$, and $d = 0.8$ at $\phi = 0.2$ in Figs. 2(a) and 2(b), respectively, using the full expression derived from Eq. (9). The aforementioned features agree well with the numerical results. The example of $\phi = 0.2$ shows the ability to tune the heights of the potential barriers from symmetric into asymmetric.

In addition, we note that for any function $f(x) \approx (x - x_{\min})^n/\epsilon$ for $n > 1$ (integers), the corresponding geometric potential can be a double barrier centered at $x = x_{\min}$ since $f'(x_{\min}) = 0$. Here, we have provided a simple realization of nonadiabatic potential double barriers, making them drastically different from those in the case of $f(x) \approx x/\epsilon$ [35–37,47]. Our method does not require lattice modulation [38–40] or atomic levels with multi-Λ configurations [29,35].

B. Multiple barrier with subwavelength spacing

As another example, we would like to show a three-peak nonadiabatic potential. To see this, we consider the spatial function $f(x) = \frac{1+\cos(kx)}{1+\cos(kx+\phi)}$, where $\Omega_c(x) = \Omega_0[1 + \cos(kx)]$ and $\Omega_p(x) = \Omega_0[1 + \cos(kx + \phi)]$. Here the only control parameter is the phase ϕ. We derive

$$\alpha'(x) = k\frac{\sin(kx + \phi) - \sin kx + \sin\phi}{(1 + \cos kx)^2 + [1 + \cos(kx + \phi)]^2}. \tag{11}$$

By examining the properties of $\alpha'(x)$, we find the spatial features of $U_0(x)$ as follows:

(1) A central peak at $x_c = \frac{\pi}{k} - \frac{\phi}{2k}$ with $U_0(x_c) = \frac{8\hbar^2 k^2}{m\phi^2}$.

(2) Two dips at $x_{\min} = x_c \pm \frac{\phi}{2k}$ with $U_0(x_{\min}) = 0$.

(3) Two lower peaks at maximum at $x_{\max} = x_c \pm \frac{\phi}{k}$ with $U_0(x_{\max}) = \frac{9\hbar^2 k^2}{200m\phi^2}$.

We plot both the ground-state population P_{g_1} and the geometric potential $U_0(x)$ as a function of x for different values of ϕ in Fig. 3. Two flat regions in the population correspond to the dips in $U_0(x)$ and the large slope corresponds to the central peak in $U_0(x)$.

We note that the double-well potential looks similar to the plot in the right-upper panel in Fig. 3(b) in Ref. [37], but they are of different natures. Here the potential is a characteristic of the spatially varying Rabi frequencies and the state is completely dark, while the one in Ref. [37] is due to the off-resonant Raman lasers so the resulting potential is not completely dark.

The nonadiabatic multiple barriers are important in two ways. First, they provide a subwavelength potential landscape. Quasibound states and resonant tunnelings of multibarrier potentials can be studied using Wentzel-Kramers-Brillouin approximation [48,49]. Second, the subwavelength features of the multiple barriers may permit the study of enhanced dipole-dipole interactions between atoms.

IV. APPLICATION: BOUND STATES

We now discuss a study of many-body physics permitted by nonadiabatic potential barriers. The spatially varying dark state may allow the atoms to have spatially dependent magnetic moments [2] in the subwavelength regime, leading to strong magnetic dipole-dipole interactions. For concreteness, we assume the magnetic moments are aligned perpendicular to the x axis that the atoms are located at. (The situation on transverse position distribution will be discussed later.) The strength of the magnetic moment of an atom is taken to be $\mu(x) = \mu_m[2P_{g_1}(x) - 1]$, which depends on the state (spin) of the atom, i.e., $P_{g_1}(x)$. For the situation of two atoms, the total Hamiltonian is given by [35]

$$\mathcal{H}_{MB} = \frac{p_1^2}{2m} + \frac{p_2^2}{2m} + U_0(x_1) + U_0(x_2) + \frac{\mu_0\mu(x_1)\mu(x_2)}{4\pi|x_1 - x_2|^3}, \tag{12}$$

where μ_0 is the vacuum permeability, and x_i and p_i are the position and the momentum of the ith atom.

In the case of the double barriers, the atoms repel each other through the magnetic dipolar interaction if they both stay in the well. Thus a bound state can not be formed. Instead, a bound state can be formed if only one atom sits inside the well. The condition for the bound state is $E_{\min} + \frac{\mu_0\mu(x_1)\mu(x_2)}{4\pi|x_1-x_2|^3} < 0$, where $E_{\min}$ is the minimum energy of the atom inside the potential well and the energy of the other atom outside the well is neglected. By considering the size of the potential well and using the uncertainty principle, we estimate $E_{\min} \approx \hbar^2k^2/[2m\epsilon(1-d)]$. Then we estimate the minimum magnetic moment to form a bound state and we find that the required dipolar length $a_{dd} \equiv \mu_0\mu^2 m/(12\pi\hbar^2)$ [50] is on the order of the typical subwavelength spacing, i.e., $a_{dd}^{\min} \sim 0.2\sqrt{\epsilon(1-d)}\lambda \sim \Delta x$.

A more rigorous determination of $a_{dd}^{\min}$ can be obtained by numerically solving the Schördinger Eq. (12) to have at least one negative eigenvalue. The numerical calculations are performed in the region of $[0, \lambda]$, considering the periodicity of the potential and assuming both atoms are within this region. In practice, the dipole-dipole interaction would be modified due to the transverse distribution, and so does $a_{dd}^{\min}$. The dipolar potential in 3D is given by $V_{3D} = \mu_0\mu(x_1)\mu(x_2)(r^2 - 3z_{12})/(4\pi r^5)$ [51]. Here r is the interatomic distance in 3D, and z_{12} is the interatomic distance along the z axis, where the dipoles are assumed to be oriented. We assume that each atom is strongly confined in the transverse direction, where its distribution probability for the jth atom is given by $P(y_j, z_j) = \exp[-(y_j^2 + z_j^2)/l_T^2]/(\pi l_T^2)$ with l_T the strength ofthe transverse confinement. We first find the effective dipole-dipole interaction by integrating the transverse variables in V_{3D} using $P(y_j, z_j)$, and then solve Eq. (12) using the effective interaction.

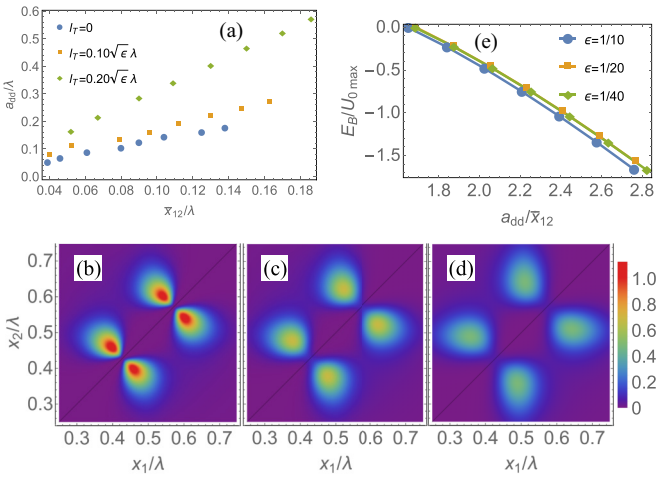

FIG. 4. (a) The minimum values of the dipolar length $a_{dd}^{\min}$ versus the average interatomic distance $\bar{x}_{12}$ for different strengths of transverse confinement l_T. For each value of confinement, $\bar{x}_{12}$ is evaluated numerically from the corresponding wave function $\psi(x_1, x_2)$, solved using $a_{dd}^{\min}$ with $\epsilon = 1/120, 1/70, 1/40, 1/28, 1/20, 1/15, 1/12, 1/10$ at $d = 0$. Density plots of $|\psi(x_1, x_2)|^2$ for (b) $l_T = 0$, (c) $l_T = 0.10\sqrt{\epsilon}\lambda$, (d) $l_T = 0.20\sqrt{\epsilon}\lambda$ using $a_{dd}^{\min}$ with $\epsilon = 1/10$. (e) Lowest bound-state eigenenergies as a function of dipolar length a_{dd} for $l_T = 0.10\sqrt{\epsilon}\lambda$ at different values of ϵ.

We study the dependence of $a_{dd}^{\min}$ shown in Fig. 4(a). In the ideal case when $l_T = 0$, we search $a_{dd}^{\min}$ for different values of ϵ (circular points). Using the critical values of a_{dd}, we calculate the average interatomic distance along the x axis $\bar{x}_{12}$ from the wave function $\psi(x_1, x_2)$. We find that $a_{dd}^{\min}$ increases linearly with $\bar{x}_{12}$ as we change ϵ, i.e., $a_{dd}^{\min} \approx 1.2\bar{x}_{12} \approx 0.55\sqrt{\epsilon}\lambda$, which is close to the value obtained in the analytical method when $d = 0$. For $l_T = 0.10\sqrt{\epsilon}\lambda \ll \bar{x}_{12}$, we find both $\bar{x}_{12}$ and $a_{dd}^{\min}$ increase slightly where $a_{dd}^{\min} \approx 1.5\bar{x}_{12}$ (square points). For $l_T = 0.20\sqrt{\epsilon}\lambda \approx \bar{x}_{12}/3$, $a_{dd}^{\min}$ is increased to about $3.0\bar{x}_{12}$ (diamond points).

We plot the bound-state probability distributions $|\psi(x_1, x_2)|^2$ using $a_{dd}^{\min}$ at $\epsilon = 1/10$ for $l_T = 0$, $0.10\sqrt{\epsilon}\lambda$, $0.20\sqrt{\epsilon}\lambda$ in Figs. 4(b)–4(d). We observe that there is a high probability to find one atom located inside the potential well while the other is outside, so the magnetic moments tend to be close to its maximum magnitude μ_m. There is almost zero probability to find atoms sitting close to the domain walls ($x_j \approx 4.25$ and 5.75) where $\mu(x)$ changes signs [35], so the contact interaction due to s-wave scattering [50] can be neglected. We further plot the lowest bound-state eigenenergies E_B as a function of a_{dd} for $\epsilon = 1/10, 1/20, 1/40$ at the transverse confinement $l_T = 0.10\sqrt{\epsilon}\lambda$ in Fig. 4(e). Eignenergies on the order of $U_{0\max}$ can be achieved with moderate dipolar length $a_{dd} \sim 2\bar{x}_{12}$. Interestingly, in the rescaled axes ($a_{dd}/\bar{x}_{12}$ and $E_B/U_{0\max}$), the dependence of eigenergies on a_{dd} has a universal relation for a fixed transverse confinement.

We also investigate the nonadiabatic potential experienced by the bound-state atoms. Due to the double-barrier potential, the average off-diagonal coupling rate can be

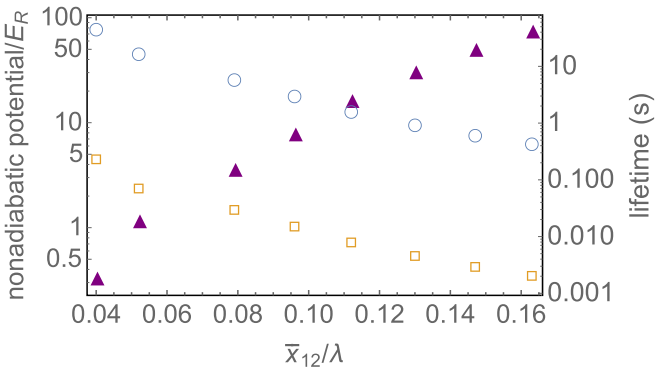

FIG. 5. The average nonadiabatic potential of a bound-state atom (open squares), the maximum potential of the double barriers (circles), and the lifetime of the bound states (triangles), versus the mean interatomic distance with the same set of ϵ in Fig. 4(a) for $l_T = 0.1\sqrt{\epsilon}\lambda$ (see text for details).

very small, which is given by $\int V_{\pm D}(x_1)|\psi(x_1,x_2)|^2 dx_1 dx_2 \leqslant \int \sqrt{U_0(x_1)U_1(x_2)}/(2\hbar)\psi(x_1,x_2)|^2 dx_1 dx_2 \equiv \bar{U}_{\rm off}/\hbar$. In Fig. 5 (empty squares), we plot this upper bound of the average off-diagonal coupling potential $\bar{U}_{\rm off}$ versus the mean interatomic distance as ϵ varies. The results show that $\bar{U}_{\rm off} \sim E_R$, which is two orders of magnitude smaller than the peak nonadiabatic potential $U_0(x_{\rm max})$ in Fig. 5 (circles). The small off-diagonal coupling potential can support very long lifetimes of the bound states. We estimate the lifetime of the bound states as $\tau = 1/\bar{\gamma}_d$, where $\bar{\gamma}_d = \gamma \int U_0(x_1)U_1(x_2)/(2\hbar\Omega(x_1))^2|\psi(x_1,x_2)|^2 dx_1 dx_2$. Using the parameters in Sec. V, we show that lifetimes on the order of seconds can be realized at tens of nanometers interatomic distances.

Moreover, the double-barrier potential can lead to bound states of three atoms known as trimers. Our trimer has one atom inside the well and two outside on each side of the barrier. Similarly, bound states can be formed in the case of the triple potential barriers. The atoms attract each other if they are separated by the center barrier such that the dipoles are opposite and the magnitude is about μ_m (Fig. 3). With periodic potentials, our multiple barriers can be interesting for the study of many-body physics in band structures, which is out of the scope of this paper.

V. EXPERIMENTAL IMPLEMENTATIONS

The nonadiabatic potential multiple barriers require the Λ atomic configuration and spatial control on the Rabi frequencies. The Λ atomic configurations have been frequently used in electromagnetic-induced transparency [45] and coherent population transfer [52]. The first experiment on nonadiabatic potentials has been performed using an ultracold ^{171}Yb gas [37] with hyperfine-split ground states.

The spatial dependence on the Rabi frequencies $\Omega_c(x)$ and $\Omega_p(x)$ is of the form $a + b\cos(kx)$, which can be realized by superposing a standing wave and a propagating wave derived from the same laser. Thus, the spatial function $f(x)$ is insensitive to the laser intensity fluctuation. As the perfect spatial function may be a challenge in experiment, a double barrier can be more easily demonstrated with an approximated function $f(x) = (x - x_{\rm min})^2/\epsilon$ by shaping the coupling and the probe lasers.

We can determine the minimum barrier spacing from $U_0(x) \ll \hbar|\Omega(x)|$. The minimum value of the Rabi frequency is $\Omega(x) = \sqrt{\Omega_c^2(x) + \Omega_p^2(x)} \approx \Omega_0\epsilon(1-d)$ for the double-barrier potentials, and $\Omega(x) \approx \Omega_0[1 - \cos^2(\phi)] \approx \Omega_0\phi^2/2$ for the triple-barrier potentials. Considering $\Omega_0 = 2\pi \times 100\,{\rm MHz}$, $\lambda = 532$ nm, and $U_0(x) \leqslant \hbar|\Omega(x)|/5$ for ^{171}Yb atoms, we obtain the minimum barrier spacing to be 13 nm and 24 nm for the double-barrier potentials and the triple-barrier potentials, respectively. The corresponding minimum energy inside the double barriers is $E_{\rm min}/\hbar \approx 2\pi \times 280\,{\rm kHz}$. We estimate the maximum excitation probability is $P_B \approx 4\%$. Taking $\gamma = 2\pi \times 182\,{\rm kHz}$ [37], we find the scattering rate on the dark states through the open channel is about $2\pi \times 7\,{\rm kHz}$. In the above analysis, we assumed $|\Delta| \lesssim |\Omega(x)|$, however, for larger single-photon detunings, the laser intensities need to be stronger to get the same subwavelength feature without breaking the BO approximations.

VI. CONCLUSION

In this paper, we presented a method of creating nonadiabatic potentials of multiple barriers separated at tens of nanometers via spatial engineering of the laser intensities. The ability of spatial control could potentially open a direction to engineer interesting subwavelength potential landscapes. We studied several concrete examples on realizing subwavelength multiple barriers and their application for bound states. Interestingly, we show that double-barrier potentials can support bound states of very long lifetimes.

The multiple barriers can be a platform for the study of many-body interactions in cold atoms enhanced by the subwavelength features. This scheme may also allow further studies on trapping atoms without the conventional optical dipole potentials and super-resolution quantum microscopy [53,54].

ACKNOWLEDGMENT

This research is supported by a grant from King Abdulaziz City for Science and Technology (KACST).

[1] I. Bloch, Nat. Phys. **1**, 23 (2005).
[2] I. Bloch, J. Dalibard, and W. Zwerger, Rev. Mod. Phys. **80**, 885 (2008).
[3] R. Grimm, M. Weidemüller, Y. B. Ovchinnikov, B. Bederson, and H. Walther, Optical dipole traps for neutral atoms, *Advances In Atomic, Molecular, and Optical Physics*, Vol. 42 (Academic Press, 2000), pp. 95–170.
[4] D. E. Chang, J. D. Thompson, H. Park, V. Vuletić, A. S. Zibrov, P. Zoller, and M. D. Lukin, Phys. Rev. Lett. **103**, 123004 (2009).

[5] M. Gullans, T. G. Tiecke, D. E. Chang, J. Feist, J. D. Thompson, J. I. Cirac, P. Zoller, and M. D. Lukin, Phys. Rev. Lett. **109**, 235309 (2012).

[6] O. Romero-Isart, C. Navau, A. Sanchez, P. Zoller, and J. I. Cirac, Phys. Rev. Lett. **111**, 145304 (2013).

[7] J. D. Thompson, T. G. Tiecke, N. P. de Leon, J. Feist, A. V. Akimov, M. Gullans, A. S. Zibrov, V. Vuletić, and M. D. Lukin, Science **340**, 1202 (2013).

[8] R. Mitsch, C. Sayrin, B. Albrecht, P. Schneeweiss, and A. Rauschenbeutel, Nat. Commun. **5**, 5713 (2014).

[9] A. González-Tudela, C. L. Hung, D. E. Chang, J. I. Cirac, and H. J. Kimble, Nat. Photonics **9**, 320 (2015).

[10] B. Brezger, T. Schulze, P. O. Schmidt, R. M. T. Pfau, and J. Mlynek, Europhys. Lett. **46**, 148 (1999).

[11] F. M. Huang and N. I. Zheludev, Nano Lett. **9**, 1249 (2009).

[12] J. R. Gardner, M. L. Marable, G. R. Welch, and J. E. Thomas, Phys. Rev. Lett. **70**, 3404 (1993).

[13] Y. Qi, F. Zhou, T. Huang, Y. Niu, and S. Gong, J. Mod. Opt. **59**, 1092 (2012).

[14] D. D. Yavuz, N. A. Proite, and J. T. Green, Phys. Rev. A **79**, 055401 (2009).

[15] Z. Liao, M. Al-Amri, and M. Suhail Zubairy, Phys. Rev. Lett. **105**, 183601 (2010).

[16] Q. Sun, M. Al-Amri, M. O. Scully, and M. S. Zubairy, Phys. Rev. A **83**, 063818 (2011).

[17] S. Nascimbene, N. Goldman, N. R. Cooper, and J. Dalibard, Phys. Rev. Lett. **115**, 140401 (2015).

[18] W. Yi, A. J. Daley, G. Pupillo, and P. Zoller, New J. Phys. **10**, 073015 (2008).

[19] N. Lundblad, P. J. Lee, I. B. Spielman, B. L. Brown, W. D. Phillips, and J. V. Porto, Phys. Rev. Lett. **100**, 150401 (2008).

[20] M. Shotter, D. Trypogeorgos, and C. Foot, Phys. Rev. A **78**, 051602(R) (2008).

[21] P. R. Berman, B. Dubetsky, and J. L. Cohen, Phys. Rev. A **58**, 4801 (1998).

[22] M. Weitz, G. Cennini, G. Ritt, and C. Geckeler, Phys. Rev. A **70**, 043414 (2004).

[23] T. Salger, C. Geckeler, S. Kling, and M. Weitz, Phys. Rev. Lett. **99**, 190405 (2007).

[24] W. Ge, P. R. Hemmer, and M. S. Zubairy, Phys. Rev. A **87**, 023818 (2013).

[25] M. Sahrai, H. Tajalli, K. T. Kapale, and M. S. Zubairy, Phys. Rev. A **72**, 013820 (2005).

[26] G. S. Agarwal and K. T. Kapale, J. Phys. B: At. Mol. Opt. Phys., **39**, 3437 (2006).

[27] D. D. Yavuz and N. A. Proite, Phys. Rev. A **76**, 041802(R) (2007).

[28] A. V. Gorshkov, L. Jiang, M. Greiner, P. Zoller, and M. D. Lukin, Phys. Rev. Lett. **100**, 093005 (2008).

[29] M. Kiffner, J. Evers, and M. S. Zubairy, Phys. Rev. Lett. **100**, 073602 (2008).

[30] H. Li, V. A. Sautenkov, M. M. Kash, A. V. Sokolov, G. R. Welch, Y. V. Rostovtsev, M. S. Zubairy, and M. O. Scully, Phys. Rev. A **78**, 013803 (2008).

[31] J. Mompart, V. Ahufinger, and G. Birkl, Phys. Rev. A **79**, 053638 (2009).

[32] D. Viscor, J. L. Rubio, G. Birkl, J. Mompart, and V. Ahufinger, Phys. Rev. A **86**, 063409 (2012).

[33] J. A. Miles, Z. J. Simmons, and D. D. Yavuz, Phys. Rev. X **3**, 031014 (2013).

[34] R. Dum and M. Olshanii, Phys. Rev. Lett. **76**, 1788 (1996).

[35] M. Lacki, M. A. Baranov, H. Pichler, and P. Zoller, Phys. Rev. Lett. **117**, 233001 (2016).

[36] F. Jendrzejewski, S. Eckel, T. G. Tiecke, G. Juzeliūnas, G. K. Campbell, L. Jiang, and A. V. Gorshkov, Phys. Rev. A **94**, 063422 (2016).

[37] Y. Wang, S. Subhankar, P. Bienias, M. Lacki, T.-C. Tsui, M. A. Baranov, A. V. Gorshkov, P. Zoller, J. V. Porto, and S. L. Rolston, Phys. Rev. Lett. **120**, 083601 (2018).

[38] S. Subhankar, P. Bienias, P. Titum, T. Tsui, Y. Wang, A. Gorshkov, S. Rolston, and J. Porto, New J. Phys. **21**, 113058 (2019).

[39] M. Lacki, P. Zoller, and M. Baranov, Phys. Rev. A **100**, 033610 (2019).

[40] T. Tsui, Y. Wang, S. Subhankar, J. Porto, and S. Rolston, arXiv:1911.00394.

[41] V. J. Goldman, D. C. Tsui, and J. E. Cunningham, Phys. Rev. B **36**, 7635 (1987).

[42] A. G. Petukhov, A. N. Chantis, and D. O. Demchenko, Phys. Rev. Lett. **89**, 107205 (2002).

[43] R. Songmuang, G. Katsaros, E. Monroy, P. Spathis, C. Bougerol, M. Mongillo, and S. De Franceschi, Nano Lett. **10**, 3545 (2010).

[44] H. C. Nguyen, M. T. Hoang, and V. L. Nguyen, Phys. Rev. B **79**, 035411 (2009).

[45] M. Fleischhauer, A. Imamoglu, and J. P. Marangos, Rev. Mod. Phys. **77**, 633 (2005).

[46] M. O. Scully and M. S. Zubairy, *Quantum Optics* (Cambridge University Press, England, 1999).

[47] P. Bienias, S. Subhankar, Y. Wang, T. Tsui, F. Jendrzejewski, T. Tiecke, G. Juzeliunas, L. Jiang, S. Rolston, J. Porto *et al.*, arXiv:1808.02487.

[48] A. Modinos and N. Nicolaou, Surf. Sci. **17**, 359 (1969).

[49] A. Dutt and S. Kar, Am. J. Phys. **78**, 1352 (2010).

[50] T. Lahaye, C. Menotti, L. Santos, M. Lewenstein, and T. Pfau, Rep. Prog. Phys. **72**, 126401 (2009).

[51] H. P. Büchler, E. Demler, M. Lukin, A. Micheli, N. Prokof'ev, G. Pupillo, and P. Zoller, Phys. Rev. Lett. **98**, 060404 (2007).

[52] K. Bergmann, H. Theuer, and B. W. Shore, Rev. Mod. Phys. **70**, 1003 (1998).

[53] M. McDonald, J. Trisnadi, K.-X. Yao, and C. Chin, Phys. Rev. X **9**, 021001 (2019).

[54] S. Subhankar, Y. Wang, T.-C. Tsui, S. L. Rolston, and J. V. Porto, Phys. Rev. X **9**, 021002 (2019).